Growth of emergent simple pseudo-binary ferroelectrics and their potential in neuromorphic computing devices

Ampattu R. Jayakrishnan,†[ab] Ji S. Kim,†[c] Markus Hellenbrand, [ID][c] Luís S. Marques,[ab] Judith L. MacManus-Driscoll*[c] and José P. B. Silva [ID] *[ab]

Ferroelectric memory devices such as ferroelectric memristors, ferroelectric tunnel junctions, and field-effect transistors are considered among the most promising candidates for neuromorphic computing devices. The promise arises from their defect-independent switching mechanism, low energy consumption and high power efficiency, and important properties being aimed for are reliable switching at high speed, excellent endurance, retention, and compatibility with complementary metal–oxide–semiconductor (CMOS) technology. Binary or doped binary materials have emerged over conventional complex-composition ferroelectrics as an optimum solution, particularly in terms of CMOS compatibility. The current state-of-the-art route to achieving superlative ferroelectric performance of binary oxides is to induce ferroelectricity at the nanoscale, *e.g.*, in ultra-thin films of doped HfO_2, ZrO_2, $Zn_{1-x}Mg_xO$, $Al_{1-x}Sc_xN$, and $Bi_{1-x}Sm_xO_3$. This short review article focuses on the materials science of emerging new ferroelectric materials, including their different properties such as remanent polarization, coercive field, endurance, *etc.* The potential of these materials is discussed for neuromorphic applications.

Wider impact

Ferroelectric memory devices are considered among the most promising candidates for neuromorphic computing. The promise arises from their defect-independent switching mechanism, low energy consumption and high power efficiency, and important properties being aimed for are reliable switching at high speed, excellent endurance, retention, and compatibility with complementary metal–oxide–semiconductor (CMOS) technology, making them one of the most suitable candidates for neuroinspired computing applications. In this short review article we highlight the materials science of emerging new ferroelectric materials, such as doped HfO_2, ZrO_2, $Zn_{1-x}Mg_xO$, $Al_{1-x}Sc_xN$, and $Bi_{1-x}Sm_xO_3$, including their different properties such as remanent polarisation, coercive field, endurance, *etc.* The potential of these materials is emphasized for neuromorphic applications, particularly in terms of CMOS compatibility. We also discuss possible routes for materials optimization to achieve superior neuromorphic performance.

1. Neuromorphic computing and the promise of ferroelectric devices

Owing to the exponential increase in the quantity of information to be stored and processed,[1–4] there is a need for lower energy, faster and more cost-effective computing. To achieve this, new computing paradigms are highly sought after. The conventional von Neumann architecture, which is currently required to perform processing of large quantities of data, leads to low energy efficiency attributable to the separation of processing and memory units, which leads to a high energy cost when moving data back and forth between the two.[3,4] The imminent end of Moore's Law will also limit computing capacity. Although in its early stage, neuromorphic, 'brain-like', computing has received significant attention as a possible alternative for undertaking data-intensive cognitive tasks quickly and efficiently. In neuromorphic computing systems, the two key structures are artificial neural network (ANN) and spiking neural network (SNN) systems to process and store information in the same place, thus eliminating the energy-intensive data shuttling between the two.[2–4] An analog synaptic device can be used to emulate the synaptic functionality in ANNs or SNNs for realizing cognitive tasks such as parallel computation and adaptive learning.[3,4] The analog synaptic device is crucial in neuromorphic computing as a device with an effectively

[a] Physics Center of Minho and Porto Universities (CF-UM-UP), University of Minho, Campus de Gualtar, 4710-057 Braga, Portugal. E-mail: josesilva@fisica.uminho.pt

[b] Laboratory of Physics for Materials and Emergent Technologies, LapMET, University of Minho, 4710-057 Braga, Portugal

[c] Dept. of Materials Science and Metallurgy, University of Cambridge, 27 Charles Babbage Rd., Cambridge, CB3 0FS, UK. E-mail: jld35@cam.ac.uk

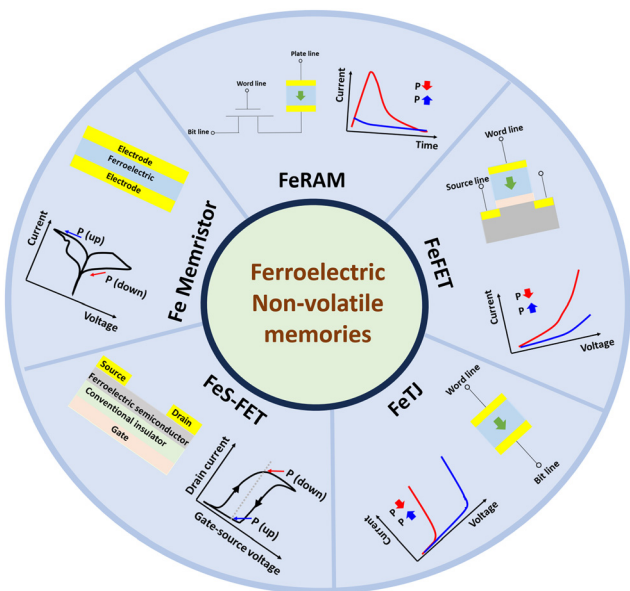† These authors contributed equally to this work.

Fig. 1 Different types of ferroelectric non-volatile memories that are applicable to neuromorphic computing and their corresponding current responses.

Fig. 2 Publications per year based on ferroelectric memories from the year 1998 up to 2023 [Analyze Results (webofscience.com)].

controllable conductance, which can be successfully arranged in a crossbar array to execute 'neural' tasks such as matrix vector multiplication. A multi-level non-volatile memory element can be used as an analog synaptic device and has the potential to implement potentiation (ability to gradually increase the conductance upon voltage pulses) and depression (ability to gradually decrease the conductance upon voltage pulses) for short-term and long-term plasticity. Non-volatile memory (NVM) devices can be based on resistive switching, phase change, and magnetic and ferroelectric materials, amongst others, and can imitate synapses by using just a single device or a few devices. Among them, ferroelectric-material-based memories such as ferroelectric random access memory (FeRAM), ferroelectric field-effect transistors (FeFETs, FETs with ferroelectric gate dielectrics), ferroelectric semiconductor field-effect transistors (FeS-FETs, FETs with ferroelectric semiconductor channels), ferroelectric tunnel junctions (FeTJs), and ferroelectric memristors (Fe memristors) are the most promising contenders owing to their inherent benefits such as a defect-independent switching mechanism, low energy consumption, and good power efficiency for neuromorphic computing systems.[4–6] Fig. 1 provides a schematic to illustrate the structures and functionalities of these devices.

2. Evolution of ferroelectric materials for non-volatile memory devices

In the electronics area, recent applications include ferroelectric non-volatile memory devices, which can be considered as the basic building blocks for neuromorphic computing devices.[4,7,8] Ferroelectric materials possess the ability to switch, upon appropriate voltage application, the polarization direction of their rem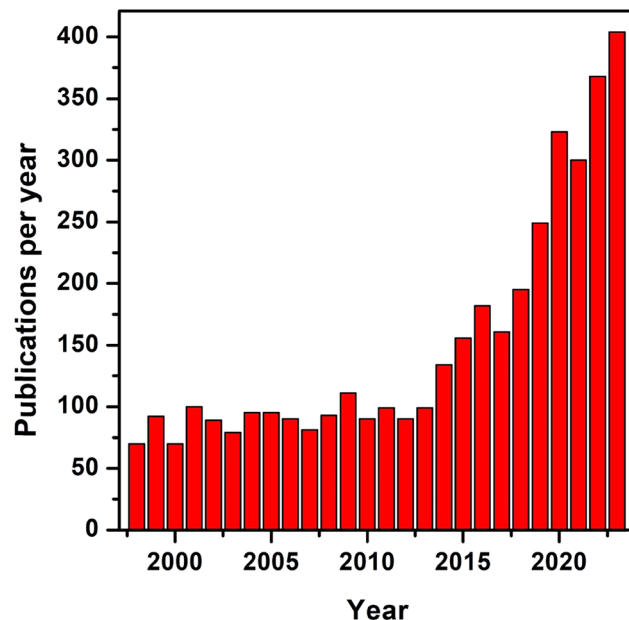anent polarization (P_r), which is stable at zero electric field. This offers features like fast read/write speed, low power consumption, and high reliability compared with conventional floating-gate electrically erasable programmable read-only memory (EEPROM) and flash EEPROM devices, which require long read/write times and high voltages.[8] Furthermore, ferroelectric materials can offer unique gradual domain switching characteristics, which provide the aforementioned multi-level conductance/resistance functionality. As a result, there is an increased interest in ferroelectric materials for non-volatile memory and neuromorphic applications. Fig. 2 shows the evolution of the number of publications per year since 1998, using the keywords 'ferroelectric materials and memory applications' in a Web of Science search. Up to 2013, the number of publications remained almost constant and then increased exponentially. This is linked to the discovery of new ferroelectric materials, as discussed below.

Perovskite-based ferroelectric materials such as lead zirconate titanate (PZT) and strontium bismuth tantalate (SBT) are promising materials for achieving the performance required for memory applications such as logic-in memory (LiM) and non-volatile logic devices.[9–17] For instance, different companies (such as Cypress Semiconductor, Texas Instruments, and Fujitsu) installed a PZT-based FeRAM in applications, including wearable medical gadgets, smart cards, energy meters, airplane black boxes, radio frequency tags, and code storage in microcontrollers.[11] SBT-based FeFETs with a huge memory window and almost infinite cycling endurance ($>10^{12}$) were demonstrated by Sakai et al.,[12] which later exhibited adequate operation in non-volatile logic (NVL) circuits[12] and 64 kbit NAND memory arrays.[13] However, while recent investigations concentrated on the continued physical scaling-down of the metal–oxide–semiconductor field-effect transistor (MOSFET),[13,15] the integration of perovskite oxides with front-end semiconductor manufacturing processes faced difficulties,

particularly those related to perovskite etching, high crystallization temperature, hydrogen sensitivity, thickness, and cell size scaling beyond the 130 nm technology node.[9,11] For instance, PZT experiences scalability problems,[9,11] because it often loses its polarization in thin films at the nanoscale due to large depolarization fields. Increasingly, 3D integration is required for high-density memory technology with constantly decreasing dimensions, which exacerbates the scaling difficulties for perovskite ferroelectric films at the industrial level.[11] Furthermore, PZT contains lead, which makes it toxic with serious health implications.

Considering the aforementioned challenges of perovskites, the discovery of ferroelectricity in Si-doped hafnium oxide (Si:HfO$_2$) thin films has provided a promising alternative to resolve these problems.[15,16] Following this exciting discovery, ferroelectricity in the nano-regime in Si:HfO$_2$ has attracted significant attention from the ferroelectrics community due to its compatibility with the complementary metal–oxide–semiconductor (CMOS) technology. Inducing ferroelectricity at the nanoscale is the current trend in non-volatile memories to realize applications such as high-density memory, storage class memory, neuromorphic computing, hardware security, etc.[17] Recent progress in this field has introduced new ferroelectric materials besides Si:HfO$_2$ with promising ferroelectric polarization and superior scalability to the nanoscale regime that are compatible with CMOS for the next-generation ferroelectric memories as shown in Fig. 3.[18–34] Fig. 3 also provides some keywords for the enhancement of P_r with moderate coercive field (E_c) values (1–2 MV cm^{-1}), which can induce large memory windows in non-volatile memory devices such as FeFETs for non-destructive

readout operations.[1] For FeFETs, however, a moderate P_r is already ideal, as too high of a P_r value can deteriorate the device reliability due to a high depolarization field and a high concentration of trapped charges.[1] Fig. 3 clearly provides a picture that orthorhombic (o-) Hf$_{0.5}$Zr$_{0.5}$O$_2$ is at an advanced stage compared with other ferroelectric materials in terms of achieving good P_r, low E_c, and excellent CMOS compatibility. Table 1 complements Fig. 3, showing further details such as preparation methods, electrode materials, and film thicknesses, which were used in the ferroelectric-based devices, together with other relevant key ferroelectric performance indicators such as required wake-up cycles (the number of switching cycles required to achieve the maximum P_r), endurance, Curie temperature (T_c), etc. With this as the background, this short review focuses on the breakthroughs in the newly introduced ferroelectric materials from the viewpoint of their ferroelectric properties and how they are beneficial for neuromorphic applications. Finally, we conclude the review article with a perspective on this burgeoning area.

3. Novel ferroelectric materials for neuromorphics

3.1 HfO$_2$ and ZrO$_2$-based films

Since the discovery of ferroelectricity in Si-doped hafnium oxide in 2011, doped hafnium oxide has been receiving significant attention.[35] The discovery of CMOS-compatible and scalable ferroelectric materials has excited the ferroelectrics community.[35,36] Following this, there have been extensive investigations into its fundamentals and applications. Hafnium oxide typically adopts a stable monoclinic phase ($P2_1/c$) at room temperature, a tetragonal ($P4_2/mnc$) structure at >2100 K, and a cubic ($Fm\bar{3}m$) structure at >2800 K.[35,36] These phases are non-polar, i.e., non-ferroelectric. So far, there have been a tremendous number of studies, experimental and computational, investigating the stabilization of meta-stable polar phases. Ferroelectricity in hafnium- and zirconium-based oxides arises from meta-stable, polar orthorhombic (o-) or rhombohedral (r-) phases with space groups $Pca2_1$ or $R3m$.[22,37] In addition, several factors including doping, deposition method, post-deposition treatment, interface chemistry, etc. have shown to enhance the ferroelectric performance of these materials.[38–40] In terms of doping, numerous dopants have been investigated such as Si, La, Gd, Y, Sr, Al, and Zr.[38–47] Out of all the dopants in hafnium oxide, zirconium shows the most promise owing to the robust ferroelectric properties upon introducing it. Wei et al. reported wake-up-free ferroelectric switching in ultra-thin Hf$_{0.5}$Zr$_{0.5}$O$_2$ films (thickness of 5 nm) by stabilizing the ferroelectric r-phase using a compressive epitaxial strain engineering strategy.[22] Recently, the same group reported that the polarization switching in r-phase Hf$_{0.5}$Zr$_{0.5}$O$_2$ films (thickness of 6 nm) might be ascribed to reversible oxygen vacancy migration.[45] In another work, Stylianidis et al. reported ferroelectricity in 5-nm-thick Hf$_{0.5}$Zr$_{0.5}$O$_2$ films also attributable to the polarization switching driven by oxygen vacancy migration.[46] Yun et al., on the other hand, confirmed polarization switching in yttrium-doped HfO$_2$ with an o-phase with a small rhombohedral
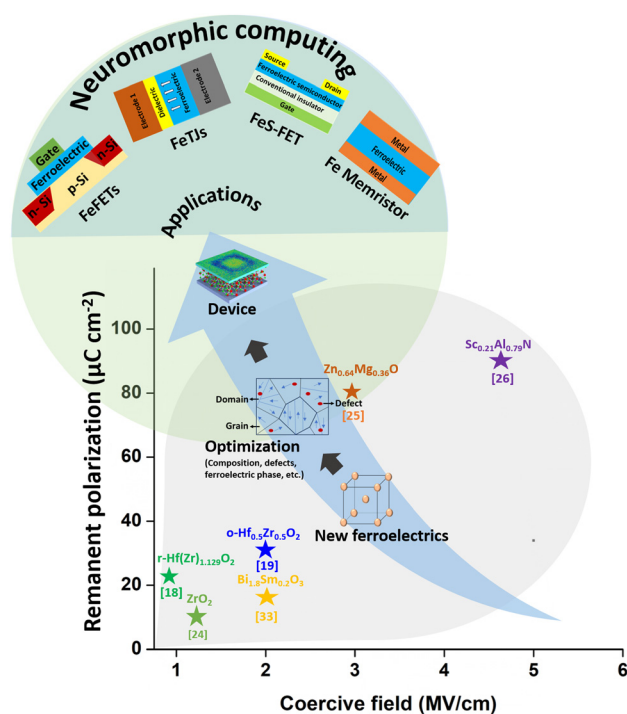

Fig. 3 New ferroelectric materials and their possible applications. o- and r- indicate orthorhombic and rhombohedral phases, respectively.

Table 1 Key reports on (pseudo-)binary ferroelectric materials and their properties

Material and thickness	Method	P_r (μC cm^{-2})	E_c (MV cm^{-1})	T_c (K)	Wake-up (cycle)	Endurance (cycles)	Top/bottom electrodes	Substrate	Ref.
Hf(Zr)$_{1.129}$O$_2$ (12 nm)	Sputtering	22	0.65	—	None	10^{12}	TiN (top and bottom)	Si	18
Hf$_{0.5}$Zr$_{0.5}$O$_2$ (20 nm)	ALD	~1.07	~19	—	Needed	10^4	Ni/Pt	SiO$_2$/Si	19
Hf$_{0.5}$Zr$_{0.5}$O$_2$ (10 nm)	ALD	~30	~2	—	None	10^4	W (top and bottom)	SiO$_2$/Si	19
Hf$_{0.5}$Zr$_{0.5}$O$_2$ (11 nm)	Sputtering	~1	~10	—	Needed	10^4	TiN/Pt	SiO$_2$/Si	20
Hf$_{0.5}$Zr$_{0.5}$O$_2$ (9 nm)	ALD	~1	~21.7	—	Needed	10^5	TiN/Pt	SiO$_2$/Si	21
Hf$_{0.5}$Zr$_{0.5}$O$_2$ (5 nm)	PLD	~5	~34	—	None	—	La$_{0.7}$Sr$_{0.3}$MnO$_3$ (top and bottom)	SrTiO$_3$	22
ZrO$_2$ (30 nm)	CVM	8.5	—	—	—	10^3	TiN/Pt	Si (100)	23
ZrO$_2$ (8 nm)	IBSD	9.3	1.2	—	None	10^6	Au (top)	Nb:SrTiO$_3$	24
Zn$_{0.64}$Mg$_{0.36}$O (300 nm)	Sputtering	80	3	—	20	10^3	Pt (top and bottom)	SiO$_2$/Si	25
Al$_{0.79}$Sc$_{0.21}$N (100 nm)	MBE	90	4.6	—	—	10^5	Au/n-type GaN	Si	26
Al$_{0.7}$Sc$_{0.30}$N (45 nm)	Sputtering	100	>5	—	—	—	TiN (top and bottom)	SiO$_2$/Si	27
Al$_{0.64}$Sc$_{0.36}$N (30 nm)	Sputtering	100	>6	—	—	<10^5	TiN (top and bottom)	SiO$_2$/Si	28
Al$_{0.64}$Sc$_{0.36}$N (16 nm)	Sputtering	30	6.5	—	—	—	Pt (top and bottom)	SiO$_2$/Si	29
Sc$_{0.30}$Al$_{0.7}$N (5 nm)	MBE	23	>6	—	—	—	Mo (top and bottom)	Mo	30
Al$_{0.72}$Sc$_{0.28}$N (5 nm)	PVD	>100	9.2	—	—	—	Al (top and bottom)	Sapphire	31
Al$_{0.64}$Sc$_{0.36}$N (100 nm)	Sputtering	80	2	—	—	10^4	Ti–Au/Pt	Si	32
Bi$_{1.8}$Sm$_{0.2}$O$_3$ (1 nm)	Sol–gel	17	~2	473	—	10^8	Au (top)	Nb:SrTiO$_3$	33
Bi$_{1.8}$Sm$_{0.2}$O$_3$ (4.6 nm)	CSM	50	0.75	—	—	10^9	Au/Cr (top)	Nb:SrTiO$_3$	34

*PLD – pulsed laser deposition, ALD – atomic layer deposition, IBSD – ion bean sputtering deposition, MBE – molecular beam epitaxy, PVD – physical vapor deposition, and CSM – chemical solution method

distortion attributable to "true" ferroelectricity, i.e., the reversible switching of the material's unit cell polarization.[47] The electrical switchability of the yttrium-doped HfO$_2$ films studied using piezo-response force microscopy revealed features of "intrinsic" ferroelectricity not obscured by extrinsic factors like charge injection. Overall, the phenomenon of ferroelectric switching in hafnia-based films is still under debate regarding the origin of the observed polarization switching.[45,46] The minimum film thickness that demonstrated ferroelectricity in Zr-doped HfO$_2$ (Hf$_{1-x}$Zr$_x$O$_2$) with x = 0.2 was 1 nm, which was grown by low-temperature atomic layer deposition (ALD) on a silicon substrate, followed by rapid thermal annealing.[48] Furthermore, the Zr-doped composition Hf$_{1-x}$Zr$_x$O$_2$, with x = 0.5, is the most promising one for its excellent ferroelectric properties attributable to the stable ferroelectric orthorhombic phase ($Pbc2_1$) due to the ferroelectric phase transition in the HfO$_2$–ZrO$_2$ solid solution.[38]

There have been many attempts to deposit ferroelectric Hf$_{0.5}$Zr$_{0.5}$O$_2$ (HZO) using various deposition techniques such as ALD, pulsed laser deposition (PLD), metal–organic chemical vapor deposition (MOCVD), or sputtering.[49–56] In the early stages of research, most HZO films were deposited using ALD on top of Si, SiO$_2$ or TiN, followed by a rapid thermal annealing (RTA) step.[39–41] Generally, an E_c value of ~1 MV cm^{-1} and a remanent polarization P_r value of >15 μC cm^{-2} were achieved.[45,47] ALD-grown HZO films tend to demonstrate wake-up behavior, which means that they require a number of applied voltage cycles prior to the actual demonstration of ferroelectric behavior or before reaching their maximum P_r value. There have been multiple attempts to mitigate this wake-up effect and some reports demonstrated wake-up-free ALD-grown HZO through capping electrode engineering, mechanical stress, and plasma treatment.[10] Furthermore, epitaxial HZO has been investigated, mainly using PLD. While PLD is currently not CMOS-compatible like ALD, it enables understanding of fundamental properties about the origin of ferroelectricity in HZO with highly crystallized single-phase films. HZO films have been grown on SrTiO$_3$ (STO) (001) with the La$_{0.67}$Sr$_{0.33}$MnO$_3$ (LSMO) buffer layer[55–58] and they typically demonstrate o-(111) oriented films. However, in 2018, Y. Wei et al. reported r-(111) ferroelectric films for the first time.[28] The factors determining the formation of a specific ferroelectric phase remain unclear. Recent studies conducted by S. Estandia et al., 2021,[57] and S. Shi et al., 2023,[58] have highlighted the significant role of the bottom electrode in achieving the ferroelectric o-phase. Their findings indicate that MnO termination of LSMO is necessary for the formation of the o-phase. Epitaxial o-HZO films tend to have a high E_c of >3 MV cm^{-1} (depending on their thickness) and P_r > 30 μC cm^{-2}. It is unclear at present which termination or other structural aspects of LSMO are needed to achieve the r-phase. In addition, recently, magnetron-sputtered r-Hf(Zr$_{1.129}$)O$_2$ films have shown a very good P_r of 22 μC cm^{-2}, an ultra-low E_c of 0.65 MV cm^{-1}, and stable performance up to ~10^{12} cycles, which seem to solve the problem of high E_c in o-phase HfO$_2$-based films. The demonstrated stabilization of the r-phase and its associated ferroelectric properties are attributed to intercalated atoms that expand the lattice, thereby increasing both in-plane and out-of-plane stresses, thus creating a more highly polarised structure, which is easier to switch due to its lower kinetic energy barrier between the two spontaneous polarization states.[18]

Rapid development of nanoscale HfO$_2$-based materials with excellent ferroelectric properties and available multi-level conductance states, along with their physical dimensions and compatibility with CMOS technology, has inspired the adoption of these materials into synaptic devices with low footprints and high energy efficiency.[49–56] The key parameters that determine the ideal requirement for a synaptic device are high P_r, moderate E_c, large on/off ratio, long cycling endurance, prolonged retention, and well-spaced conductance levels.[4] For instance, ferroelectric materials can achieve multi-level P_r states by varying the

applied electric switching field. Not only that, these materials maintain each state even after removal of the electric field. This multi-level P_r can be used to modulate the conductance of the synaptic device.[59,60] The low E_c can extend the endurance lifetime and result in low-voltage switching for non-volatile memories.[61] A large on/off ratio potentially increases the number of multi-level states by providing a large memory window.[4,62] Moreover, the endurance and retention of the ferroelectric materials allow the memory device to store the data over a long time.[62] Therefore, we can say that ferroelectric-based non-volatile memory devices are promising for synaptic elements in neuromorphic computing.

Recently, researchers have reported analog synaptic transistors based on HfO₂- and ZrO₂-based ferroelectric materials,

which employ a variety of channel materials, including WO_x, indium gallium zinc oxide (IGZO), indium zinc tin oxide (IZTO), poly-GeSn, and WS_2.[63–69] HfO₂- and ZrO₂-based ferroelectric materials are attractive due to their ferroelectricity in ultra-thin films (from ∼1 up to 10 nm) with improved reliability, low programming voltage and CMOS compatibility.[63–66] For instance, Halter *et al.* studied an $Hf_{0.57}Zr_{0.43}O_2$ thin-film-based (thickness ∼9.6 nm) FeFET with WO_x as the channel material for synaptic elements.[63] This work showcased an $Hf_{0.57}Zr_{0.43}O_2/WO_x$ stack as an FeFET with good voltage control and strong linearity and symmetry in potentiation and depression at different voltage amplitudes with identical pulse trains, which facilitate facile programming of learning algorithms. The FeFET has a short programming time of 40 ns and a low write
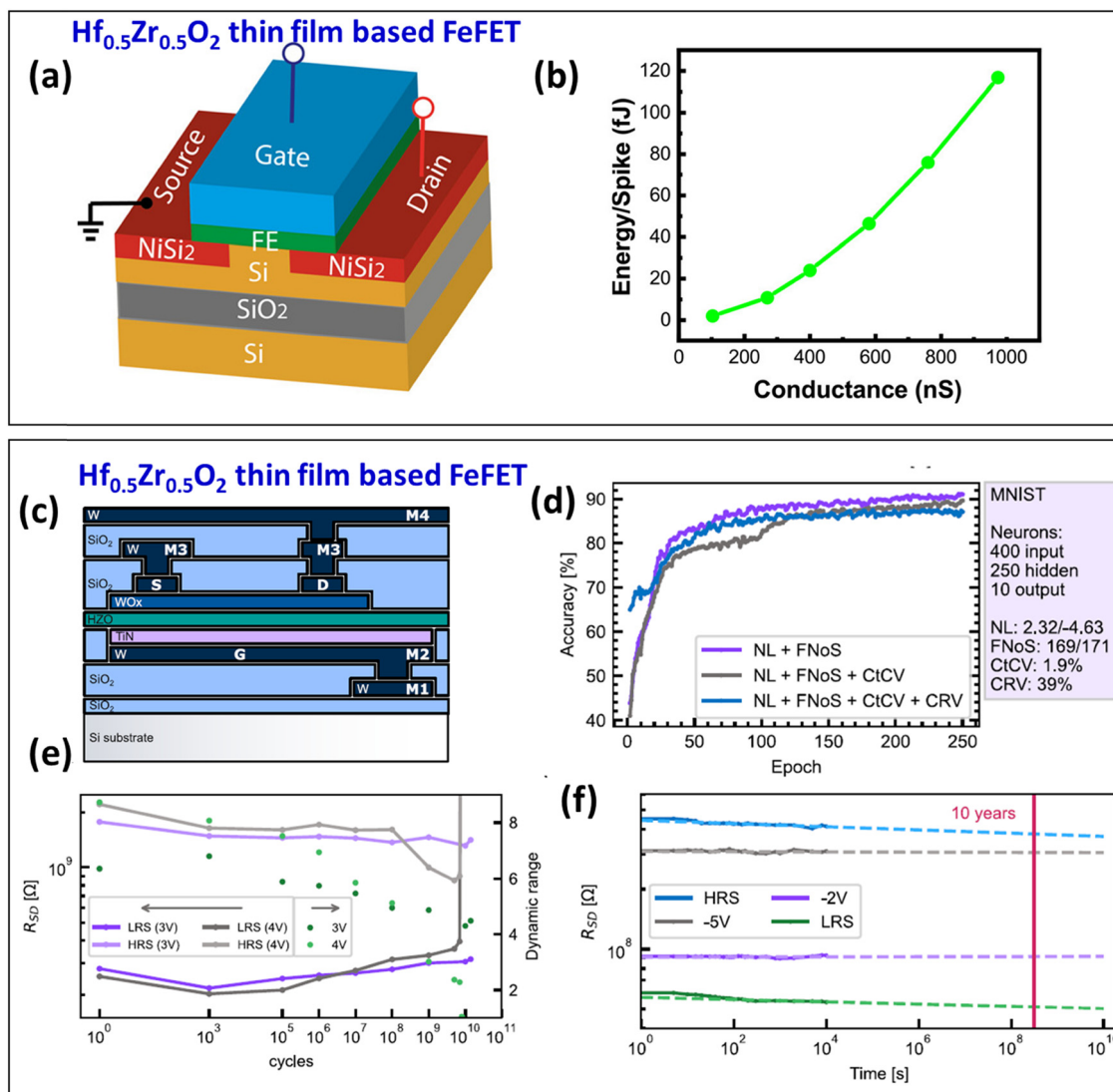
Fig. 4 (a) Schematic diagram of an $Hf_{0.5}Zr_{0.5}O_2$ thin-film-based 3-terminal FeFET. (b) Calculated energy/spike consumption at different voltage pulse amplitudes.[68] Copyright (2020) by American Chemical Society. (c) Illustration of an FeFET device based on an $Hf_{0.5}Zr_{0.5}O_2$ thin film with source (S), drain (D), gate (G), WO_x channels, ferroelectric gate dielectric, access metal lines (M1, M2), plus S access metal line (M3) and D access metal line (M4). (d) MNIST classification performance of the FeFET with different degrees of non-idealities included: non-linearity factors and finite number of steps (purple), added cycle to cycle variation (grey), and added conductance range variation (blue). (e) Endurance measurement of the FeFET at 100 kHz. (f) Retention measurements at room temperature for the four programmed states[69] with extrapolation to 10 years.

energy (2.1×10^{-17} J μm^{-2}). Furthermore, it offers multi-level programming spanning more than 4 bit depth and a stable retention over 1500 s. Moreover, the device is compatible with a back end of line (BEOL) integration into standard CMOS processes. Kim et al. reported Al-doped HfO_2 with improved switching speed (~ 107 mV per decade) and a good on/off ratio (1×10^3), demonstrating its use as a potential synaptic transistor.[65] By varying the amplitude and number of input pulses, this work was able to achieve potentiation/depression weight updates with minimal cycle-to-cycle variability and good linearity. With the performance data of this FeFET, a simulated pattern recognition accuracy of almost 90% was achieved for the Modified National Institute of Standard and Technology (MNIST) handwritten data set under optimal potentiation/depression conditions. Furthermore, Al-doped HfO_2 suppresses electrically active charge traps typically arising from the direct deposition of HfO_2 on Si and favors analog conduction modulation at low operating voltages.

Bégon-Lours et al. developed a 3.5-nm-thick $Hf_{0.5}Zr_{0.5}O_2$ thin film transistor with an on/off ratio of 7 and a small device-to-device variability ($<5\%$) suitable for neural network inference.[67] Furthermore, the device operates in the ohmic regime for the read-out, which is good for analog vector-matrix multiplication. The conduction modulation in the transistor may have originated from the motion of trapped hydrogen in the lattice and/or oxygen vacancies that form during ALD fabrication. These defects modify the conduction band energy profile and transport properties upon polarization switching. As a synaptic element, this transistor demonstrated a training accuracy of 92% after 36 epochs on the MNIST data set. Xi et al. experimentally demonstrated a CMOS-compatible FeFET using an $Hf_{0.5}Zr_{0.5}O_2$ ferroelectric layer (thickness ~ 10 nm, Fig. 4(a)) with a very high on/off ratio (3×10^4) and low write energy consumption (~ 2 fJ) at low voltages (0.5 V) (Fig. 4(b)).[68] This synaptic device was based on $Hf_{0.5}Zr_{0.5}O_2/NiSi_2/$Si and used partial polarization switching to modulate the Schottky barrier of the $NiSi_2$/Si contacts for analog conduction modulation with symmetric potentiation/depression characteristics and high retention.

Very recently, Halter et al. reported an $Hf_{0.5}Zr_{0.5}O_2$ thin film FeFET (thickness ~ 10 nm) (Fig. 4(c)) with good P_r (~ 14 μC cm^{-2}) and a very low write energy (1.2 fJ) at higher voltages (6 V).[69] In terms of neuromorphic behavior, using the NeuroSim framework, a good MNIST classification accuracy of 88% was achieved (Fig. 4(d)) due to fine-grained, quasi-continuous monotonic resistance changes with more than 200 steps between the low and high resistance states and a low cycle-to-cycle variability. Furthermore, a very minimal dynamic range loss with a very high endurance ($>10^{10}$ cycles) and an outstanding retention (>10 years) was achieved (Fig. 4(e) and (f)). As a result, the FeFET is promising for neural network inference and cognitive computing.

In a different study, Mikheev et al. fabricated a p-type Si/$Hf_{0.5}Zr_{0.5}O_2$/TiN-based second-order memristor using a 4-nm-thin ferroelectric $Hf_{0.5}Zr_{0.5}O_2$ ultra-thin film to investigate the synaptic functions for neuromorphic computing.[70] In first-order memristors, the conductance is defined entirely by external stimuli and thus to emulate the temporal synapse response, an accurate overlapping of pre- and post-synaptic spikes is needed, which is not the case in biological synapses. In second-order memristors, the conductance is controlled by both the external stimuli and their instant internal state. These second-order memristors do not require particular spike shapes and their overlapping and thus allow a straightforward natural emulation of the frequency response. Mikheev et al. demonstrated conductivity (synaptic weight) modulation with $R_{OFF}/R_{ON} \sim 8$ via the gradual switching of polarization in ferroelectric domains of polycrystalline 4-nm-thin ferroelectric $Hf_{0.5}Zr_{0.5}O_2$ films. The built-in electric field and charge trapping/de-trapping at the defect states at the Si interface contribute further to the temporal behavior, expressing modulation similar to synapses in biological systems. The work of Mikheev et al. also experimentally demonstrated synaptic functions such as short-term plasticity, paired-pulse facilitation (PPF), paired-pulse depression (PPD), and spike-rate-dependent plasticity (SRDP), which are similar to biological synaptic systems. Müller et al. developed another promising approach using an Fe memristor for the prospects of neuromorphic applications. A simple metal–ferroelectric–metal (MFM) structure utilizing an ultra-thin $Hf_{0.93}Y_{0.07}O_2$ film of thickness 4.5 nm displayed a very good on/off ratio (540) and a large range of accessible resistance states for future NVM.[66] This work introduces polarization-modulated charge transport from Schottky-barrier-limited to Ohmic conduction, reporting a high on/off ratio for ultrathin epitaxial $Hf_{0.93}Y_{0.07}O_2$ films. The impact of the polarization reversal on the charge transport across a MFM device, utilizing a partially depleted insulating ferroelectric barrier, is demonstrated, which is conceptually different from those in FeTJs, where a fully depleted insulating ferroelectric barrier is used.

From these examples, it can be concluded that these HfO_2- and ZrO_2-based materials are all viable options for large-scale integration into neuromorphic hardware. However, one of the critical outstanding challenges with HfO_2 and ZrO_2 FeFETs are wake-up effects, about which no information has been provided in any of the reviewed examples.

Table 2 shows some key reports on HfO_2- and ZrO_2-based synaptic transistors, including features like P_r, endurance pulse information, write pulse duration, on/off ratio, synaptic weight, and write energy. Fig. 5 complements Table 2 in terms of the key parameters (thickness, P_r, endurance, the number of conductance levels ω, and write energy) of HfO_2- and ZrO_2-based materials for application as synaptic devices. It can be concluded that reducing the thickness of the ferroelectric layer below 10 nm causes degradation of the potentiation/depression due to increased leakage currents during the program/erase process.[4] Unfortunately, there is not much information available about the write energy and MNIST data accuracy except for $Hf_{0.5}Zr_{0.5}O_2$ thin film FeFETs, which are considered to be key neuromorphic parameters. FeS-FET device structures are not currently being investigated on a large scale, while FeTJs and Fe memristors have been scarcely investigated.

Just as with HfO_2, pure or doped ZrO_2-based thin films are promising for high-k gate dielectrics and are compatible with CMOS technology, and it is surprising that the material has

Table 2 Key reports on HfO_2- and ZrO_2-based synaptic memory devices and their properties

Device structure	P_r (μC cm^{-2})	Endurance (cycles)	Voltage range for potentiation & depression	Write pulse duration (μs)	On/off ratio	Conductance levels $\Delta \omega$ for potentiation/ depression	Write energy (fJ)	Ref.
$Al_2O_3/WO_x/Hf_{0.57}Zr_{0.43}O_2$ (9.6 nm)/TiN/Si (FeFET)	~12	10^5	1 to 3.1 V and −0.9 to −3 V (incremental)	10	1.9	22/22	—	63
$ITO/IGZO/Al:HfO_2$ (10 nm)/W/p-Si(FeFET)	~5	10^2	1.9 to 4 V and −1.2 to −3.3 V (incremental)	1	1×10^3	70/70	—	65
$W/Hf_{0.57}Zr_{0.5}O_2$ (5 nm)/n-$SrTiO_3$/Si(FeTJ)	~14	—	−2 V and 2 V (identical)	50	1.55	16/16	8	64
$TiN/Hf_{0.5}Zr_{0.5}O_2$ (3.5 nm)/WO_x/SiO_2/Si(FeFET)	~14	10^{10}	−1.4 V and 2 V (unidentical)	0.02	7	25/25	—	67
$TiN/Hf_{0.5}Zr_{0.5}O_2$(10 nm)/TiN/SiO_2/Si (FeFET)	~14	10^5	0.5 V and −0.5 V (identical)	1	3×10^4	50/50	2	68
$TiN/Hf_{0.5}Zr_{0.5}O_2$ (10 nm)/WO_x/SiO_2/Si (FeFET)	~14	10^{10}	0.6 V to 5 V and −1.25 V to −5.5 V (incremental)	500	—	171/169	1.2	69
$Au/Hf_{0.93}Y_{0.07}O_2$ (4.5 nm)/$La_{0.7}Sr_{0.3}MnO_3$/Nb–$SrTiO_3$ (Fe Memristor)	—	—	1.5 to 4 V and −1.5 to −4 V (incremental)	10 000	540	50/50	—	66

been seldom investigated for ferroelectricity.[71–74] In 2016, Fan et al. fabricated ZrO_2 films using magnetron sputtering and stabilized the ferroelectric o-phase by substrate-induced strain to form highly textured (111) ZrO_2 ferroelectric films.[72] It was found that the o-phase is stabilized by applying compressive strain along the in-plane $\langle11\bar{2}\rangle$ direction. Consequently, a phase transition from the tetragonal (t-) phase to the ferroelectric o-phase occurred in the ZrO_2 film. Lin et al. verified the existence of a ferroelectric o-phase in undoped ZrO_2 films (10 nm thick) made by remote plasma ALD.[73] More recently, Wang et al. reported a P_r of 8.5 μC cm^{-2} and a high relative permittivity of 39.6 in 30-nm-thick pure ZrO_2 films grown on Si (100) via chemical solution deposition.[23] Ferroelectricity in pure ZrO_2 films is established after a wake-up operation of about 1000 cycles. According to Wang et al., the wake-up process induces ferroelectricity by changing the non-ferroelectric t-phase to a ferroelectric o-phase via oxygen loss.

In addition, it was found that an increase in film thickness (40 nm and 50 nm) weakened the ferroelectric behavior and this was ascribed to the phase transformation from the o-phase to the cubic phase as strain relaxes with thickness. In the same year, Silva et al. showed ferroelectricity in r-phase ZrO_2 thin films without any wake-up process.[20] The films were grown on (111)-oriented Nb:$SrTiO_3$ (Nb:STO) using ion beam sputtering. Ferroelectricity in these ZrO_2 thin films is attributed to the formation of a polar r-($R3m$) phase under epitaxial compressive strain. Pole figure measurements of the 8-nm-thick ZrO_2 thin films confirmed the plane distances $d_{200} = d_{020} = d_{002}$ in the range between 2.55 Å and 2.50 Å, indicative of an r-space group. The films displayed a spontaneous polarization P_s of 20 μC cm^{-2} and a P_r of 10.8 μC cm^{-2} with an E_c of 1.5 MV cm^{-1}. By converting an anti-ferroelectric t-phase to a ferroelectric o-phase, Cheema et al. introduced a strategy to achieve ferroelectricity in ZrO_2 films through reduced dimensionality.[71] The
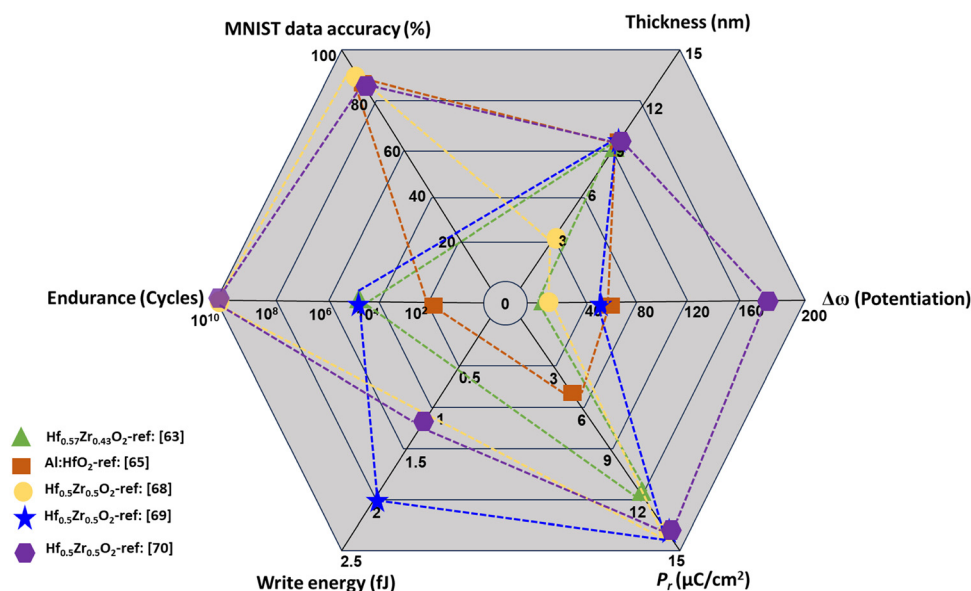
Fig. 5 Performance of HfO_2- and ZrO_2-based FeFETs for different key parameters that are required for neuromorphic computing devices.

films were deposited using ALD. This work reduced the ZrO_2 film thickness down to 5 Å and stabilized the ferroelectric o-phase. The reduced dimensionality can be achieved through hydrostatic pressure, chemical pressure, or epitaxial strain.[71] Very recently, Silva *et al.* stabilized the o-phase in 8-nm-thick ZrO_2 films deposited using ion beam sputtering on Nb:STO substrate.[20] The films displayed a P_r of 9.3 μC cm^{-2} and an E_c of 1.2 MV cm^{-1} without any wake-up process. The lack of wake-up effect is attractive for next-generation memory devices. However, the potential application of ferroelectric ZrO_2 in neuromorphics is yet to be demonstrated.

3.2 Doped zinc oxide films

ZnO is regarded as a conventional non-ferroelectric II–VI wurtzite semiconductor material with a band gap ~ 3.4 eV.[75] Theoretical investigations done by Moriwake *et al.*, however, reported the possibility of a spontaneous polarization P_s of ~ 90 μC cm^{-2} in wurtzite ZnO due to the structural distortion arising from the relative displacement of cations against anions along the *c*-axis.[75,76] This is attributed to the tensile strain experienced along the *ab*-plane along the [0001] direction. Consequently, the potential barrier obstructing the polarization rotation is reduced and the non-polar $P6_3/mmc$ switches between two equivalent polar states ($P6_3mc$), inducing ferroelectricity.[76]

In order to make ZnO attractive as a ferroelectric tunneling resistive memory for low power non-volatile memory devices with fast switching speeds, appropriate dopants such as Li, Mn, Co, Cr, and Ti are required both to tune the band gap of ZnO and to enhance its ferroelectricity.[77–79] Onodera *et al.* reported ferroelectric behavior in wurtzite-structured Li-doped ZnO bulk ceramics with a modest P_r of ~ 0.044 μC cm^{-2} at ambient temperature using *P–E* hysteresis loop measurements. Here, the Li ion occupies the off-centered positions, replacing Zn ions. This forms electric dipoles to induce ferroelectric polarization.[79] Yang *et al.* reported ferroelectric polarization in V-doped ZnO thin films deposited on Si(111) substrates with a P_r of ~ 0.2 μC cm^{-2} using magnetron co-sputtering. The introduction of V^{5+} at Zn^{2+} sites affects the 3d–2p hybridization and induces a local dipole moment by changing the Zn(v)–O bond length.[77] While the principal demonstration of ferroelectricity in ZnO is promising, the low P_r in these doped ZnO films obviously requires improvement, possibly by optimizing the dopant type and concentration and strain levels.[76–80]

Recently, Mg has emerged as an ideal stressor not only capable of inducing superior ferroelectric properties, but also capable of stabilizing the wurtzite structure of ZnO.[81–83] Jacques *et al.* reported a high P_r of ~ 80 μC cm^{-2} and an E_c of ~ 3 MV cm^{-1} for epitaxial $Zn_{0.64}Mg_{0.36}O$ (ZMO) films (thickness ~ 300 nm) deposited using magnetron sputtering with pure Zn and Mg targets.[81] To induce ferroelectric switching, an applied electric field greater than E_c had to be applied for a sufficiently long duration to wake up the polarization states. The full realization of the ferroelectric switching in ZMO films was observed after 100 cycles with the application of an electric field of ~ 5 MV cm^{-1}. The excess electric field of 5 MV cm^{-1}

had to be applied to overcome the internal electric field in the ZMO films due to increased deep trap states attributed to the migration of defects at the interfaces.[81] In $Zn_{1-x}Mg_xO$ (ZnMgO) films of ~ 500 nm thickness grown on single-crystal Al_2O_3, with x between 0.35 and 0.37, Ferri *et al.* reported ferroelectric switching with a P_r exceeding 100 μC cm^{-2} and an E_c less than 3 MV cm^{-1}.[82] The pronounced wake-up process in the ferroelectric ZnMgO films concluded after 100 cycles with an applied electric field greater than E_c. Ferri *et al.* also demonstrated the direct integration of ZnMgO films on flexible substrates such as kapton and polystyrene. This introduces the possibility of exploring, for the first time, ferroelectric switching in wurtzite solid solutions for neuromorphic computing. Despite the promising P_r values, however, a considerable decrease of E_c is needed to make ZnO realistic for neuromorphic applications. To achieve this, we anticipate that different strategies such as epitaxial growth, doping, strain engineering, domain engineering, *etc.* can be used.

3.3 Scandium-doped aluminum nitride ($Al_{1-x}Sc_xN$) films

Pure aluminum nitride (AlN) with a wurtzite structure is generally a pyroelectric material as its polarization direction cannot be switched with an applied electric field.[69] According to the literature, however, ferroelectricity in AlN can be induced by adding Sc to it. This is ascribed to the elongation of the Al–N bond parallel to the *c*-axis, which arises due to the formation of a metastable hexagonal phase introduced by Sc.[84–88] The layered hexagonal phase, particularly around the Sc site, is non-polar. The increase in the Sc content flattens the ionic potential towards the hexagonal phase and therefore reduces the energy barrier, which obstructs the polarization switching in the wurtzite structure of AlN.[84–88] As a result, Sc-doped AlN experiences ferroelectric switching.

Fichtner *et al.* reported a high P_r of ~ 100 μC cm^{-2} with an E_c of ~ 3 MV cm^{-1} in reactively sputtered $Al_{0.64}Sc_{0.36}N$ films of thickness 400 nm deposited on oxidized Si(100) wafers.[84] This excellent ferroelectricity in $Al_{0.64}Sc_{0.36}N$ is associated with the existence of the hexagonal phase and compositional homogeneity, which allows only $180°$ orientation of domains. Besides, the $Al_{0.64}Sc_{0.36}N$ film exhibits a piezoelectric coefficient of 15.7 pm V^{-1} with an excellent symmetry around the field axis. It should be noted that the increased Sc content above a particular limit causes a linear decrease in E_c. This was concluded from the composition analysis performed by Fichtner *et al.*, where exceeding a certain threshold of Sc content impeded the ferroelectric properties again, favoring the formation of more of a non-polar layered hexagonal phase, which in turn distorts the wurtzite structure due to the expansion of the basal plane and the increasing length of the metal–nitrogen bond.[84] Wang *et al.* fabricated $Al_{0.71}Sc_{0.29}N$ thin film capacitors to demonstrate ferroelectric switching.[89] The 100 nm $Al_{0.71}Sc_{0.29}N$ thin film was deposited on Pt-coated Ti using magnetron sputtering. A wake-up operation up to 50 cycles was required to grow and stabilize the ferroelectric domains in the $Al_{0.71}Sc_{0.29}N$ thin film. The $Al_{0.71}Sc_{0.29}N$ thin film displayed a P_r of ~ 100 μC cm^{-2} with an E_c of

$\sim$5.5 MV cm^{-1} near room temperature. Further work performed by Wang *et al.* reported a record high P_r of $\sim$140 μC cm^{-2} and an E_c of $\sim$6.5 MV cm^{-1} in 20-nm-thick Al$_{0.68}$Sc$_{0.32}$N thin films near room temperature.[90] The film was deposited on a Pt (111)/Ti/SiO$_2$/ Si wafer using magnetron sputtering. The formation of a strongly *c*-axis-oriented Al$_{0.68}$Sc$_{0.32}$N film was elucidated using X-ray diffraction and rocking curve measurements, which confirmed its highly crystalline nature with a full width at half maximum of 2.7°. The excellent ferroelectric switching in this Al$_{0.68}$Sc$_{0.32}$N film might be due to a combination of high crystalline nature, low film thickness, and a lower depolarization field at the surface oxide. Yasuoka *et al.* studied the effect of deposition conditions on Al$_{1-x}$Sc$_x$N thin films deposited on Pt(111)/Ti/SiO$_2$/Si substrates using magnetron sputtering.[91] The group investigated the effect of sputtering gas, film composition, and film thickness on the ferroelectric behavior of Al$_{1-x}$Sc$_x$N films. The Al$_{1-x}$Sc$_x$N films deposited under an N$_2$ atmosphere showed good ferroelectricity compared with an N$_2$ + Ar atmosphere. The smaller value of P_r in the Al$_{1-x}$Sc$_x$N film deposited under an N$_2$ + Ar atmosphere might be attributed to the increased pinning of polarization states. The composition analysis of Al$_{1-x}$Sc$_x$N films in the range $0 < x < 0.34$ displayed an increase in lattice parameter c up to 0.22 Å and showed a decreasing trend above this value. This indicates that the ferroelectricity is optimum for the composition $x = 0.22$ and is ascribed to the presence of more non-polar layered hexagonal phases for larger values of x, which contribute to the lengthening of the metal–nitrogen bond. Furthermore, the crystal structure analysis of the various thicknesses (48–140 nm) of Al$_{1-x}$Sc$_x$N films with $x = 0.22$ using rocking curve XRD analysis revealed that the preferential (002) orientation becomes predominant above 50 nm. Thus, the maximum values of P_r and the dielectric constant were found to be 129 μC cm^{-2} and 15.9, respectively, for the Al$_{1-x}$Sc$_x$N films with $x = 0.22$ and 140 nm thickness.[91] Ryoo *et al.* reported a high P_r of $\sim$100 μC cm^{-2} and an E_c of >5 MV cm^{-1} in 45-nm-thick Al$_{0.7}$Sc$_{0.3}$N films deposited on a SiO$_2$/Si substrate *via* sputtering.[27] The enhanced ferroelectricity in the Al$_{0.7}$Sc$_{0.3}$N thin films arises from the imposed compressive strain, which eventually increases the *c/a*-lattice parameter ratio attributable to the enhanced (002)-preferred orientation. In another work, Kim *et al.* fabricated 30-nm-thick Al$_{0.70}$Sc$_{0.30}$N wurtzite thin films with a high P_r of 100 μC cm^{-2} with an E_c of >6 MV cm^{-1} *via* sputtering deposition on a SiO$_2$/Si substrate. This is ascribed to the highly *c*-axis-oriented crystal structure of the film favouring very good switching speed, eliminating the slow motion of the domain wall. Furthermore, a fatigue-free behavior ($<10^5$ cycles) was observed in the film.[28] Musavigharavi *et al.* grew 20-nm-thick ferroelectric Al$_{0.64}$Sc$_{0.36}$N on a SiO$_2$/Si substrate by sputtering. The work reported a maximum P_r of 30 μC cm^{-2} with an E_c of 6.5 MV cm^{-1}. The large polarization is attributed to the formation of a highly crystalline wurtzite structure of Al$_{0.64}$Sc$_{0.36}$N at lower thickness with a preferential (002) orientation achieved normal to the SiO$_2$/Si substrate.[29] Wang *et al.*, in 2023, reported ferroelectricity in ultra-thin Al$_{0.7}$Sc$_{0.3}$N deposited on a molybdenum (Mo) substrate using molecular beam epitaxy (MBE). The work displayed a P_r of 23 μC cm^{-2} with an E_c of >6 MV cm^{-1}.[30] The group investigated the ferroelectric behavior of Al$_{0.7}$Sc$_{0.3}$N by varying the

thickness from 100 to 5 nm. It is observed that the thickness decrease had a significant effect on P_r (decreases) and E_c (increases). The diminution in the ferroelectric polarization in the wurtzite Al$_{0.7}$Sc$_{0.3}$N ultra-thin films results from the high compressive strain induced by the scaling-down of the film thickness. Furthermore, in addition to the Janovec–Kay–Dunn (JKD) model (where E_c is proportional to $d^{-2/3}$ with the film thickness d), the formation of a non-switchable "dead" layer or dielectric interfacial layer, or a finite screening length of the electrodes, contributes to the increase in E_c with the scaling down of the thickness. Zheng *et al.* developed ultra-thin Al$_{0.72}$Sc$_{0.28}$N films (thickness $\sim$5 nm) deposited on a sapphire substrate using physical vapor deposition and investigated their ferroelectric properties. The work showed $P_r > 100$ μC cm^{-2} with E_c $\sim$9.2 MV cm^{-1}.[31] This work suggests that the high E_c value for lower thickness may be due to the decrease in the *c/a* ratio arising from the Sc alloying ratio or from the film stress. Liu *et al.* fabricated an FeFET device, as shown in Fig. 6(a), composed of 100-nm-thick sputtered Al$_{0.71}$Sc$_{0.29}$N integrated with a two-dimensional (2D) molybdenum disulfide (MoS$_2$) channel.[32] The device achieved a high P_r of 80 μC cm^{-2} and an E_c of 6 MV cm^{-1}. Furthermore, the device exhibited an excellent on/off ratio of $\sim$10^6, an endurance of 10^4 cycles, and a good retention of 10^5 s, which was however measured at a gate voltage of $\pm$40 V, which is a very high writing voltage (Fig. 6(b)). The 2D MoS$_2$ channel minimizes the depolarization field by compensating the incomplete charge induced by the ferroelectric Al$_{0.71}$Sc$_{0.29}$N layer, consequently providing prolonged retention and minimal read-disturb. Very recently, Wang *et al.* studied the ferroelectric and analog resistive switching of memristors in 5 nm wurtzite Al$_{0.7}$Sc$_{0.3}$N with gallium nitride (GaN) as the semiconductor channel grown on a sapphire substrate using MBE, as shown in Fig. 6(c).[92] The device demonstrated its potential as a candidate for nonlinear ferroelectric resistive memory arrays with a high on/ off ratio of 10^5, an endurance of $>10^4$ cycles, and a good retention of 10^5 s. Furthermore, the work displayed eight conductance states during potentiation and depression for the incremental pulse scheme with voltages ranging from -7.6 V to -8.24 V and 1.9 V to 3.564 V, respectively. However, some reports suggest that a minimum of ten conductance states during potentiation/depression are required for the effective training process by an ANN in the analog domain.[92] Nevertheless, the device yielded a recognition accuracy of 92.9% from MNIST simulation (Fig. 6(d)).

Based on these promising demonstrations, we foresee that more studies on these high-P_r Al$_{1-x}$Sc$_x$N films could produce further synaptic elements with multi-level polarization states essential for analog conduction modulation during potentiation/depression with CMOS compatibility. Strategies like domain and strain engineering, as well as thickness reduction, could potentially be explored for reducing E_c to enhance the potential neuromorphic applicability.

3.4 Layered bismuth oxide films

Bismuth oxide is a classical ferroelectric material with a very high Curie temperature ($\sim$673 K) and excellent cycling endurance ($\sim$10^{12} cycles).[93,94] This discovery builds on the finding of
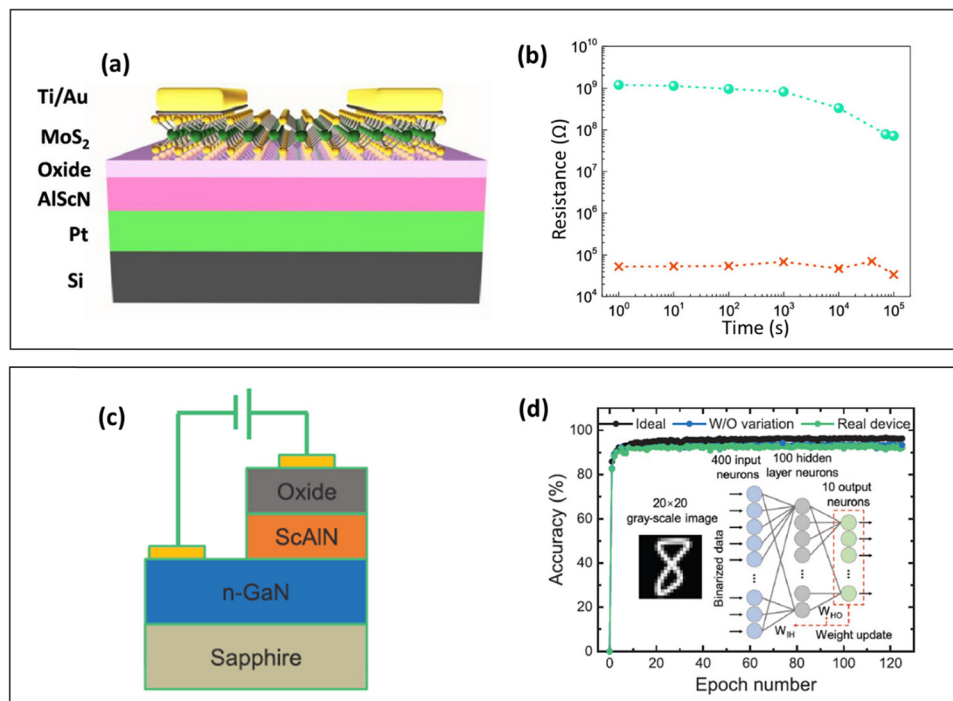
Fig. 6 (a) Schematic diagram of a 100-nm-thick ferroelectric AlScN–MoS$_2$ FeFET and (b) retention measurements made by monitoring the drain current at various time intervals of up to 100 000 s with a gate voltage of ±40 V. Copyright (2020) by American Chemical Society.[32] (c) Illustration of an Fe memristor device using an AlScN ultra-thin film. (d) MNIST simulated classification performance of the AlScN Fe memristor showing the best recognition accuracy of 92.9% with non-linearity and cycle-to-cycle/device-to-device variations.[92]

in-plane ferroelectricity in BiO layers in complex layered bismuth oxide compositions, *e.g.*, Bi$_2$AlMnO$_6$ and Bi$_2$NiMnO$_6$. In these materials, the growth of the layered structure occurs more in the horizontal than in the vertical direction. It is reported that out-of-plane ferroelectric properties offer higher polarization switching than the in-plane orientation due to more uniform grains and ordered domains.[95–98] Very recently, Yang *et al.* reported strong out-of-plane ferroelectricity in 1-nm-thin Sm-substituted bismuth oxide (Bi$_{1.8}$Sm$_{0.2}$O$_3$) grown on an Al$_2$O$_3$ substrate using sol–gel spin-coating.[99] The 1-nm-thin Bi$_{1.8}$Sm$_{0.2}$O$_3$ (BSO) film exhibited a P_r of 17 μC cm^{-2}, which is high compared with other ultra-thin films such as HZO,

CuInP$_2$S$_6$, BaTiO$_3$, BiFeO$_3$, and PbZr$_{0.2}$Ti$_{0.8}$O$_3$. Here, the Bi layers at the interface serve as strain bearers to relax the lattice mismatch from the substrate, thus maintaining an unstrained growth of the film. Even though the reduced thickness affects the ferroelectricity in the BSO film due to surface charges and leakage, the remarkable P_r arises due to the incorporation of the Sm dopants, which preserves the ferroelectric phase in the BSO and maintains a high polarization by suppressing the depolarization field. Furthermore, Sm promotes the tolerance of the layered Bi structure to uphold the stability of the ferroelectric structure at low dimensions. A slightly thicker film of 4.56-nm-thin BSO displayed a high P_r of 50 μC cm^{-2} with an E_c
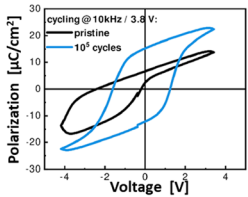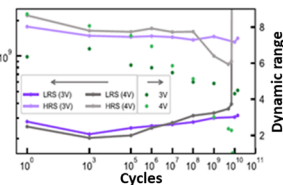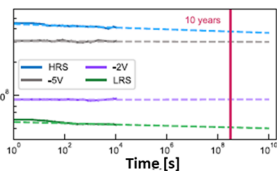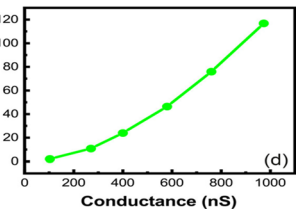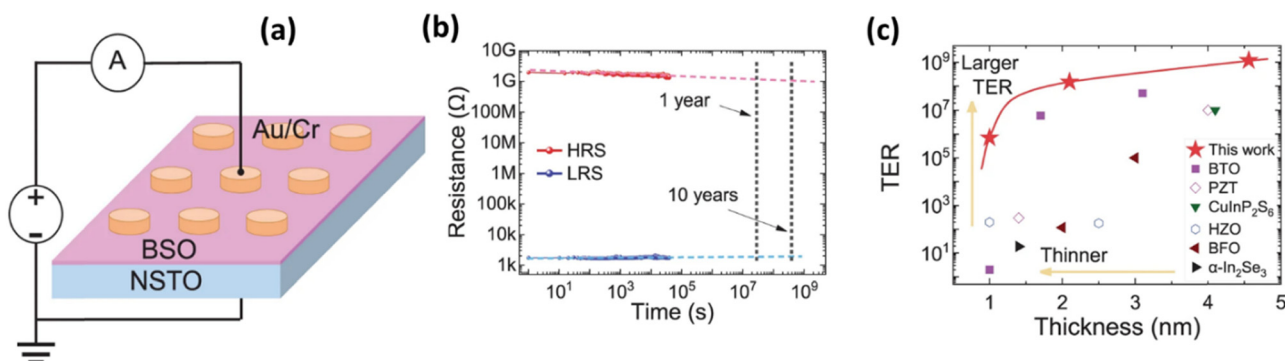

Fig. 7 (a) Schematic diagram of a 4.6-nm-thin ferroelectric Bi$_{1.8}$Sm$_{0.2}$O$_3$ (BSO) FeTJ device structure and (b) retention measurement indicating prolonged retention for more than 10 years by extrapolation. (c) Comparison of tunnelling electroresistance (TER) values of the BSO FTJ device with other ferroelectric materials and thicknesses.[34]

Table 3 Important performance parameters for achieving neuromorphic functionality for the different materials. For each material, we have selected the best-performing single device based on P_r and E_c values, and the other entries in each column are for the same device. Illustrative figures for each parameter are taken from ref. 20, 25, 34, 69, and 92. Here, the tick sign indicates that the ferroelectric material meets each particular parameter requirement for neuromorphics, the cross sign means the performance has not been reached and a dash means that the parameters have not yet been explored

Parameter	$Hf_{0.5}Zr_{0.5}O_2$ [70]	ZrO_2 [20]	$Zn_{0.64}Mg_{0.36}O$ [25]	$Sc_{0.21}Al_{0.79}N$ [93]	$Bi_{1.8}Sm_{0.2}O_3$ [34]
P_r (>10 μC/cm²) & E_c (~1-2 MV/cm)	✓	✗	✗	✓	✓
Endurance (>10⁵ Cycles)	✓	✓	✗	✓	✓
Retention (10 Years)	✓	—	—	✓	✓
Write energy (<2 fJ)	✓	—	—	—	—
Wake-up effect (free)	—	—	—	—	—
Imprint effect (free)	—	—	—	—	—
Operating voltage (<1V)	✗	—	—	—	—
On/Off ratio (>=10)	✓	—	—	✓	—
Plasticity and linearity (>8 bit memory and 526 individual resistance levels)	✗	—	—	—	—
d2d and c2c variability (<=2% tolerable)	—	—	—	—	—

of about 0.75 MV cm^{-1}. In addition, the film exhibited an excellent cycling endurance ($\sim 10^8$ cycles) and outstanding thermal stability (up to 493 K). The demonstrated E_c and P_r values at highly scaled film thicknesses are promising for neuromorphic applications such as non-destructive read/write operations and synaptic functionality. Hence, this new material warrants further deeper explorative studies of its neuromorphic behavior.

Very recently, Gia *et al.* demonstrated an FeTJ based on an ultra-thin BSO film of thickness 4.6 nm deposited on Nb:STO using a chemical solution method (Fig. 7(a)).[34] The FeTJ exhibited long retention time (10 years, Fig. 7(b)) and exceptional cycling endurance (10^9). The stable tetragonal-like phase induced by Sm substitution provided prolonged retention in the BSO-based FeTJs by reducing the depolarization field. Furthermore, the BSO film showed an excellent P_r of 50 μC cm^{-2} and a very low E_c of 0.75 MV cm^{-1}. Moreover, the FeTJ displayed a large tunnelling electroresistance compared to other materials attributable to the large polarization maintained at the minute thickness (Fig. 7(c)). Consequently, both the ferroelectric barrier height and barrier width at the depletion region surface of Nb:STO were modulated. In this work, a single BSO-based FeTJ demonstrated 32 conductance states without any write-termination process. Hence, this new material warrants further deeper explorative studies of its neuromorphic behavior.

A summary comparing P_r, E_c, endurance, retention, and write energy of the different materials, together with neuromorphic performance parameters, is shown in Table 3. It is possible to conclude that $Hf_{0.5}Zr_{0.5}O_2$ partially meets the requirements of neuromorphic applications. In the case of $Hf_{0.5}Zr_{0.5}O_2$, we took the best performance[56] from Fig. 5 to compare the neuromorphic parameters with other materials. However, these novel ferroelectrics are in the early stage of development and strong performance improvements are eagerly anticipated.

4. Concluding remarks

The recent discoveries of ferroelectricity in binary and pseudo-binary nanoscale oxide thin films offer great possibilities for miniaturized non-volatile memory and neuromorphic computing devices. We have reviewed the most promising of these oxide thin film materials, and examples are summarized in Table 1. These new materials show high polarization in the nano-regime, which is particularly important for ultra-scaled devices. Most importantly, HfO_2- and ZrO_2-based non-volatile FeFETs have already been established as promising contenders for synaptic elements in neuromorphic devices due to their established deposition methods, high ferroelectric polarization, scalability, high endurance, defect-free operation mechanism, and CMOS compatibility.[63–68] The impressive performance of HfO_2- and ZrO_2-based thin film FeFETs is getting significant attention due to high scalability, good endurance, and CMOS compatibility.[4]

In addition, these group-IV-based oxide materials exhibit important performance metrics, including good linearity/symmetry, multilevel states, high on/off ratios and low write energy characteristics, which are desirable for neuromorphic applications.[4,63–65,67–69] However, HfO_2- and ZrO_2-based thin films typically struggle with parameters such as imprint, wake-up, fatigue, and consequently with uniform cycling endurance. Also, reducing the film thickness, as is required in some cases, may increase E_c and therefore necessitate higher operating voltages, leading to higher leakage currents during program/erase operations.

Based on the initial demonstrations of ferroelectricity in Sc-AlN, ZnMgO, and $BiSmO_3$, there is potential for these materials for neuromorphic computing, too. However, while ZnMgO exhibits exceptional P_r values comparable to HfO_2 and ZrO_2 thin films, as of yet the large coercive field and thickness of ZnMgO present challenges for its integration as a neuromorphic computing device. Also, Sc-doped AlN and ZnMgO suffer from problems of low endurance and the requirement for wake-up cycling. Furthermore, parameters like on/off ratio, potentiation/depression, write energy, synaptic weight, *etc.* remain unexplored in ferroelectric ZrO_2 and ZnMgO. Also, while very recently studied $Bi_{1−x}Sm_xO_3$[34] meets some performance parameter requirements for a synaptic element, all these performance parameters need to be explored in a substrate compatible with CMOS fabrication processes.

For all the aforementioned oxide materials, strategies should be implemented to control the ferroelectric phase stability and reduce oxygen vacancy concentrations. More studies on epitaxial films are useful in this regard as they serve as model systems to tune the structure carefully without influences of grain boundaries and mixed phases.
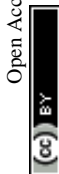
With a good understanding of the fundamental properties of materials and their control, domains can then be engineered to achieve low-voltage multi-level synaptic plasticity with low variability for neuromorphic applications. For example, the controlled design of sufficiently many domains in a thin film would allow a more fine-grained tuning of multiple polarization levels for quasi-analog synaptic plasticity and at the same time would improve variability due to the suppression of stochastic switching of only a few domains. Finally, we note that there are also many opportunities to expand the aforementioned ferroelectric thin film systems for applications beyond memory and neuromorphic computing, namely in pyroelectric- and piezoelectric-based energy harvesters, transducers, energy storage, *etc.*[100–105]

Conflicts of interest

There are no conflicts to declare.

Acknowledgements

References

1 T. Mikolajick, M. H. Park, L. Begon-Lours and S. Slesazeck, From ferroelectric material optimization to neuromorphic devices, *Adv. Mater.*, 2023, **35**(37), 2206042.

2 G. Indiveri, B. Linares-Barranco, R. Legenstein, G. Deligeorgis and T. Prodromakis, Integration of nano-scale memristor synapses in neuromorphic computing architectures, *Nanotechnology*, 2013, **24**(38), 384010.

3 M. Prezioso, F. Merrikh-Bayat, B. D. Hoskins, G. C. Adam, K. K. Likharev and D. B. Strukov, Training and operation of an integrated neuromorphic network based on metal-oxide memristors, *Nature*, 2015, **521**(7550), 61–64.

4 D. H. Lee, G. H. Park, S. H. Kim, J. Y. Park, K. Yang, S. Slesazeck, T. Mikolajick and M. H. Park, Neuromorphic devices based on fluorite-structured ferroelectrics, *InfoMat*, 2022, **4**(12), e12380.

5 T. Mikolajick, S. Slesazeck, H. Mulaosmanovic, M. H. Park, S. Fichtner, P. D. Lomenzo, M. Hoffmann and U. Schroeder, Next generation ferroelectric materials for semiconductor process integration and their applications, *J. Appl. Phys.*, 2021, **129**(10), 100901.

6 M. Si, A. K. Saha, S. Gao, G. Qiu, J. Qin, Y. Duan, J. Jian, C. Niu, H. Wang, W. Wu and S. K. Gupta, A ferroelectric semiconductor field-effect transistor, *Nat. Electron.*, 2019, **2**(12), 580–586.

7 S. Das, Z. Hong, M. McCarter, P. Shafer, Y. T. Shao, D. A. Muller, L. W. Martin and R. Ramesh, A new era in ferroelectrics, *APL Mater.*, 2020, **8**(12), 120902.

8 L. W. Martin and A. M. Rappe, Thin-film ferroelectric materials and their applications, *Nat. Rev. Mater.*, 2016, **2**(2), 1–14.

9 J. Y. Park, D. H. Choe, D. H. Lee, G. T. Yu, K. Yang, S. H. Kim, G. H. Park, S. G. Nam, H. J. Lee, S. Jo and B. J. Kuh, Revival of Ferroelectric Memories Based on Emerging Fluorite-Structured Ferroelectrics, *Adv. Mater.*, 2022, 2204904.

10 K. Yao, S. Chen, S. C. Lai and Y. M. Yousry, Enabling distributed intelligence with ferroelectric multifunctionalities, *Adv. Sci.*, 2022, **9**(1), 2103842.

11 A. I. Khan, A. Keshavarzi and S. Datta, The future of ferroelectric field-effect transistor technology, *Nat. Electron.*, 2020, **3**(10), 588–597.

12 S. Sakai and R. Ilangovan, Metal-ferroelectric-insulator-semiconductor memory FET with long retention and high endurance, *IEEE Electron Device Lett.*, 2004, **25**(6), 369–371.

13 M. Takahashi, T. Horiuchi, Q. H. Li, S. Wang, K. Y. Yun and S. Sakai, Basic operation of novel ferroelectric CMOS circuits, *Electron. Lett.*, 2008, **44**(7), 1.

14 W. Banerjee, A. Kashir and S. Kamba, Hafnium oxide (HfO_2)–a multifunctional oxide: a review on the prospect and challenges of hafnium oxide in resistive switching and ferroelectric memories, *Small*, 2022, **18**(23), 2107575.

15 J. P. Silva, R. Alcala, U. E. Avci, N. Barrett, L. Bégon-Lours, M. Borg, S. Byun, S. C. Chang, S. W. Cheong, D. H. Choe and J. Coignus, Roadmap on ferroelectric hafnia-and zirconia-based materials and devices, *APL Mater.*, 2023, **11**(8), 089201.

16 B. Noheda, P. Nukala and M. Acuautla, Lessons from hafnium dioxide-based ferroelectrics, *Nat. Mater.*, 2023, **22**(5), 562–569.

17 M. H. Park, D. Kwon, U. Schroeder and T. Mikolajick, Binary ferroelectric oxides for future computing paradigms, *MRS Bull.*, 2021, 1–9.

18 Y. Wang, L. Tao, R. Guzman, Q. Luo, W. Zhou, Y. Yang, Y. Wei, Y. Liu, P. Jiang, Y. Chen and S. Lv, A stable rhombohedral phase in ferroelectric Hf $(Zr)_{1+x}O_2$ capacitor with ultralow coercive field, *Science*, 2023, **381**(6657), 558–563.

19 Y. C. Lin, F. McGuire and A. D. Franklin, Realizing ferroelectric $Hf_{0.5}Zr_{0.5}O_2$ with elemental capping layers, *J. Vac. Sci. Technol., B: Nanotechnol. Microelectron.: Mater., Process., Meas., Phenom.*, 2018, **36**(1), 011204.

20 Y. H. Lee, H. J. Kim, T. Moon, K. Do Kim, S. D. Hyun, H. W. Park, Y. B. Lee, M. H. Park and C. S. Hwang, Preparation and characterization of ferroelectric $Hf_{0.5}Zr_{0.5}O_2$ thin films grown by reactive sputtering, *Nanotechnology*, 2017, **28**(30), 305703.

21 H. J. Kim, M. H. Park, Y. J. Kim, Y. H. Lee, T. Moon, K. Do Kim, S. D. Hyun and C. S. Hwang, A study on the wake-up effect of ferroelectric $Hf_{0.5}Zr_{0.5}O_2$ films by pulse-switching measurement, *Nanoscale*, 2016, **8**(3), 1383–1389.

22 Y. Wei, P. Nukala, M. Salverda, S. Matzen, H. J. Zhao, J. Momand, A. S. Everhardt, G. Agnus, G. R. Blake, P. Lecoeur and B. J. Kooi, A rhombohedral ferroelectric phase in epitaxially strained $Hf_{0.5}Zr_{0.5}O_2$ thin films, *Nat. Mater.*, 2018, **17**(12), 1095–1100.

23 J. Wang, D. Zhou, W. Dong, X. Hou, F. Liu, N. Sun, F. Ali and Z. Li, Ferroelectric properties of pure ZrO_2 thin films by chemical solution deposition, *Ceram. Int.*, 2021, **47**(12), 16845–16851.

24 J. P. Silva, M. C. Istrate, M. Hellenbrand, A. Jan, M. T. Becker, J. Symonowicz, F. G. Figueiras, V. Lenzi, M. O. Hill, C. Ghica and K. N. Romanyuk, Ferroelectricity and negative piezoelectric coefficient in orthorhombic phase pure ZrO_2 thin films, *Appl. Mater. Today*, 2023, **30**, 101708.

25 L. Jacques, G. Ryu, D. Goodling, S. Bachu, R. Taheri, P. Yousefian, S. Shetty, B. Akkopru-Akgun, C. Randall, N. Alem and J. P. Maria, Wake up and retention in zinc magnesium oxide ferroelectric films, *J. Appl. Phys.*, 2023, **133**(22), 224102.

26 P. Wang, D. Wang, S. Mondal and Z. Mi, Ferroelectric N-polar ScAlN/GaN heterostructures grown by molecular beam epitaxy, *Appl. Phys. Lett.*, 2022, **121**(2), 023501.

27 S. K. Ryoo, K. D. Kim, H. W. Park, Y. B. Lee, S. H. Lee, I. S. Lee, S. Byun, D. Shim, J. H. Lee, H. Kim and Y. H. Jang, Investigation of optimum deposition conditions of radio frequency reactive magnetron sputtering of $Al_{0.7}Sc_{0.3}N$ film

with thickness down to 20 nm, *Adv. Electron. Mater.*, 2022, **8**(11), 2200726.

28 K. D. Kim, Y. B. Lee, S. H. Lee, I. S. Lee, S. K. Ryoo, S. Byun, J. H. Lee, H. Kim, H. W. Park and C. S. Hwang, Evolution of the Ferroelectric Properties of AlScN Film by Electrical Cycling with an Inhomogeneous Field Distribution, *Adv. Electron. Mater.*, 2023, **9**(5), 2201142.

29 P. Musavigharavi, A. C. Meng, D. Wang, J. Zheng, A. C. Foucher, R. H. Olsson III and E. A. Stach, Nanoscale structural and chemical properties of ferroelectric aluminum scandium nitride thin films, *J. Phys. Chem. C*, 2021, **125**(26), 14394–14400.

30 D. Wang, P. Wang, S. Mondal, M. Hu, D. Wang, Y. Wu, T. Ma and Z. Mi, Thickness scaling down to 5 nm of ferroelectric ScAlN on CMOS compatible molybdenum grown by molecular beam epitaxy, *Appl. Phys. Lett.*, 2023, **122**(5), 052101.

31 J. X. Zheng, M. M. A. Fiagbenu, G. Esteves, P. Musavigharavi, A. Gunda, D. Jariwala, E. A. Stach and R. H. Olsson, Ferroelectric behavior of sputter deposited $Al_{0.72}Sc_{0.28}N$ approaching 5 nm thickness, *Appl. Phys. Lett.*, 2023, **122**(22), 222901.

32 X. Liu, D. Wang, K. H. Kim, K. Katti, J. Zheng, P. Musavigharavi, J. Miao, E. A. Stach, R. H. Olsson III and D. Jariwala, Post-CMOS compatible aluminum scandium nitride/2D channel ferroelectric field-effect-transistor memory, *Nano Lett.*, 2021, **21**(9), 3753–3761.

33 Q. Yang, J. Hu, Y. W. Fang, Y. Jia, R. Yang, S. Deng, Y. Lu, O. Dieguez, L. Fan, D. Zheng and X. Zhang, Ferroelectricity in layered bismuth oxide down to 1 nanometer, *Science*, 2023, **379**(6638), 1218–1224.

34 Y. Jia, Q. Yang, Y. W. Fang, Y. Lu, M. Xie, J. Wei, J. Tian, L. Zhang and R. Yang, Giant tunnelling electroresistance in atomic-scale ferroelectric tunnel junctions, *Nat. Commun.*, 2024, **15**(1), 693.

35 T. S. Böscke, J. Müller, D. Bräuhaus, U. Schröder and U. Böttger, Ferroelectricity in hafnium oxide thin films, *Appl. Phys. Lett.*, 2011, **99**(10), 102903.

36 G. Segantini, B. Manchon, I. Cañero Infante, M. Bugnet, R. Barhoumi, S. Nirantar, E. Mayes, P. Rojo Romeo, N. Blanchard, D. Deleruyelle and S. Sriram, Interplay between Strain and Defects at the Interfaces of Ultra-Thin $Hf_{0.5}Zr_{0.5}O_2$-Based Ferroelectric Capacitors, *Adv. Electron. Mater.*, 2023, **9**(10), 2300171.

37 J. P. Silva, R. F. Negrea, M. C. Istrate, S. Dutta, H. Aramberri, J. Íñiguez, F. G. Figueiras, C. Ghica, K. C. Sekhar and A. L. Kholkin, Wake-up free ferroelectric rhombohedral phase in epitaxially strained ZrO_2 thin films, *ACS Appl. Mater. Interfaces*, 2021, **13**(43), 51383–51392.

38 J. Muller, T. S. Boscke, U. Schroder, S. Mueller, D. Brauhaus, U. Bottger, L. Frey and T. Mikolajick, Ferroelectricity in simple binary ZrO_2 and HfO_2, *Nano Lett.*, 2012, **12**(8), 4318–4323.

39 T. S. Böscke, S. Teichert, D. Bräuhaus, J. Müller, U. Schröder, U. Böttger and T. Mikolajick, Phase

transitions in ferroelectric silicon doped hafnium oxide, *Appl. Phys. Lett.*, 2011, **99**(11), 112904.

40 D. Martin, J. Müller, T. Schenk, T. M. Arruda, A. Kumar, E. Strelcov, E. Yurchuk, S. Müller, D. Pohl, U. Schröder and S. V. Kalinin, Ferroelectricity in Si-doped HfO_2 revealed: a binary lead-free ferroelectric, *Adv. Mater.*, 2014, **26**(48), 8198–8202.

41 T. Song, H. Tan, R. Bachelet, G. Saint-Girons, I. Fina and F. Sánchez, Impact of La concentration on ferroelectricity of La-doped HfO_2 epitaxial thin films, *ACS Appl. Electron. Mater.*, 2021, **3**, 4809–4816.

42 U. Schroeder, C. Richter, M. H. Park, T. Schenk, M. Pesic, M. Hoffmann, F. P. Fengler, D. Pohl, B. Rellinghaus, C. Zhou and C. C. Chung, Lanthanum-doped hafnium oxide: a robust ferroelectric material, *Inorg. Chem.*, 2018, **57**(5), 2752–2765.

43 T. Schenk, C. M. Fancher, M. H. Park, C. Richter, C. Künneth, A. Kersch, J. L. Jones, T. Mikolajick and U. Schroeder, On the origin of the large remanent polarization in La: HfO_2, *Adv. Electron. Mater.*, 2019, **5**(12), 1900303.

44 S. Mueller, J. Mueller, A. Singh, S. Riedel, J. Sundqvist, U. Schroeder and T. Mikolajick, Incipient ferroelectricity in Al-doped HfO_2 thin films, *Adv. Funct. Mater.*, 2012, **22**(11), 2412–2417.

45 P. Nukala, M. Ahmadi, Y. Wei, S. De Graaf, E. Stylianidis, T. Chakrabortty, S. Matzen, H. W. Zandbergen, A. Björling, D. Mannix and D. Carbone, Reversible oxygen migration and phase transitions in hafnia-based ferroelectric devices, *Science*, 2021, **372**(6542), 630–635.

46 E. Stylianidis, P. Surabhi, R. Hamming-Green, M. Salverda, Y. Wei, A. Burema, S. Matzen, T. Banerjee, A. Björling, B. Mukherjee and S. Dutta, Investigating the Electromechanical Behavior of Unconventionally Ferroelectric $Hf_{0.5}Zr_{0.5}O_2$-Based Capacitors Through Operando Nanobeam X-Ray Diffraction, *Adv. Electron. Mater.*, 2023, 2201298.

47 Y. Yun, P. Buragohain, M. Li, Z. Ahmadi, Y. Zhang, X. Li, H. Wang, J. Li, P. Lu, L. Tao and H. Wang, Intrinsic ferroelectricity in Y-doped HfO_2 thin films, *Nat. Mater.*, 2022, **21**(8), 903–909.

48 S. S. Cheema, D. Kwon, N. Shanker, R. Dos Reis, S. L. Hsu, J. Xiao, H. Zhang, R. Wagner, A. Datar, M. R. McCarter and C. R. Serrao, Enhanced ferroelectricity in ultrathin films grown directly on silicon, *Nature*, 2020, **580**(7804), 478–482.

49 M. Hyuk Park, H. Joon Kim, Y. Jin Kim, T. Moon and C. Seong Hwang, The effects of crystallographic orientation and strain of thin $Hf_{0.5}Zr_{0.5}O_2$ film on its ferroelectricity, *Appl. Phys. Lett.*, 2014, **104**(7), 072901.

50 J. Lyu, I. Fina, R. Solanas, J. Fontcuberta and F. Sánchez, Robust ferroelectricity in epitaxial $Hf_{1/2}Zr_{1/2}O_2$ thin films, *Appl. Phys. Lett.*, 2018, **113**(8), 082902.

51 T. Shiraishi, K. Katayama, T. Yokouchi, T. Shimizu, T. Oikawa, O. Sakata, H. Uchida, Y. Imai, T. Kiguchi, T. J. Konno and H. Funakubo, Impact of mechanical stress

on ferroelectricity in $(Hf_{0.5}Zr_{0.5})O_2$ thin films, *Appl. Phys. Lett.*, 2016, **108**(26), 262904.

52 M. H. Park, H. J. Kim, Y. J. Kim, W. Lee, T. Moon, K. D. Kim and C. S. Hwang, Study on the degradation mechanism of the ferroelectric properties of thin $Hf_{0.5}Zr_{0.5}O_2$ films on TiN and Ir electrodes, *Appl. Phys. Lett.*, 2014, **105**(7), 072902.

53 H. J. Kim, M. H. Park, Y. J. Kim, Y. H. Lee, T. Moon, K. Do Kim, S. D. Hyun and C. S. Hwang, A study on the wake-up effect of ferroelectric $Hf_{0.5}Zr_{0.5}O_2$ films by pulse-switching measurement, *Nanoscale*, 2016, **8**(3), 1383–1389.

54 M. H. Park, H. J. Kim, Y. J. Kim, T. Moon, K. D. Kim, Y. H. Lee, S. D. Hyun and C. S. Hwang, Study on the internal field and conduction mechanism of atomic layer deposited ferroelectric $Hf_{0.5}Zr_{0.5}O_2$ thin films, *J. Mater. Chem. C*, 2015, **3**(24), 6291–6300.

55 J. Lyu, I. Fina, R. Solanas, J. Fontcuberta and F. Sánchez, Growth window of ferroelectric epitaxial $Hf_{0.5}Zr_{0.5}O_2$ thin films, *ACS Appl. Electron. Mater.*, 2019, **1**(2), 220–228.

56 S. Estandía, N. Dix, M. F. Chisholm, I. Fina and F. Sánchez, Domain-matching epitaxy of ferroelectric $Hf_{0.5}Zr_{0.5}O_2$ (111) on $La_{2/3}Sr_{1/3}MnO_3$ (001), *Cryst. Growth Des.*, 2020, **20**(6), 3801–3806.

57 S. Estandía, J. Gazquez, M. Varela, N. Dix, M. Qian, R. Solanas, I. Fina and F. Sánchez, Critical effect of the bottom electrode on the ferroelectricity of epitaxial $Hf_{0.5}Zr_{0.5}O_2$ thin films, *J. Mater. Chem. C*, 2021, **9**(10), 3486–3492.

58 S. Shi, H. Xi, T. Cao, W. Lin, Z. Liu, J. Niu, D. Lan, C. Zhou, J. Cao, H. Su and T. Zhao, Interface-engineered ferroelectricity of epitaxial $Hf_{0.5}Zr_{0.5}O_2$ thin films, *Nat. Commun.*, 2023, **14**(1), 1780.

59 Z. Fan, J. Chen and J. Wang, Ferroelectric HfO_2-based materials for next-generation ferroelectric memories, *J. Adv. Dielectr.*, 2016, **6**(02), 1630003.

60 T. Mikolajick, S. Slesazeck, M. H. Park and U. Schroeder, Ferroelectric hafnium oxide for ferroelectric random-access memories and ferroelectric field-effect transistors, *MRS Bull.*, 2018, **43**(5), 340–346.

61 F. Ali, T. Ali, D. Lehninger, A. Sünbül, A. Viegas, R. Sachdeva, A. Abbas, M. Czernohorsky and K. Seidel, Fluorite-Structured Ferroelectric and Antiferroelectric Materials: A Gateway of Miniaturized Electronic Devices, *Adv. Funct. Mater.*, 2022, **32**(27), 2201737.

62 H. Mulaosmanovic, E. T. Breyer, S. Dünkel, S. Beyer, T. Mikolajick and S. Slesazeck, Ferroelectric field-effect transistors based on HfO_2: a review, *Nanotechnology*, 2021, **32**(50), 502002.

63 M. Halter, L. Bégon-Lours, V. Bragaglia, M. Sousa, B. J. Offrein, S. Abel, M. Luisier and J. Fompeyrine, Back-end, CMOS-compatible ferroelectric field-effect transistor for synaptic weights, *ACS Appl. Mater. Interfaces*, 2020, **12**(15), 17725–17732.

64 N. Siannas, C. Zacharaki, P. Tsipas, D. J. Kim, W. Hamouda, C. Istrate, L. Pintilie, M. Schmidbauer, C. Dubourdieu and A. Dimoulas, Electronic Synapses Enabled by an Epitaxial $SrTiO_{3-\delta}/Hf_{0.5}Zr_{0.5}O_2$ Ferroelectric Field-Effect Memristor Integrated on Silicon, *Adv. Funct. Mater.*, 2024, 2311767.

65 D. Kim, Y. R. Jeon, B. Ku, C. Chung, T. H. Kim, S. Yang, U. Won, T. Jeong and C. Choi, Analog synaptic transistor with Al-doped HfO_2 ferroelectric thin film, *ACS Appl. Mater. Interfaces*, 2021, **13**(44), 52743–52753.

66 M. L. Müller, M. T. Becker, N. Strkalj and J. L. MacManus-Driscoll, Schottky-to-Ohmic switching in ferroelectric memristors based on semiconducting $Hf_{0.93}Y_{0.07}O_2$ thin films, *Appl. Phys. Lett.*, 2022, **121**(9), 093501.

67 L. Bégon-Lours, M. Halter, F. M. Puglisi, L. Benatti, D. F. Falcone, Y. Popoff, D. Dávila Pineda, M. Sousa and B. J. Offrein, Scaled, Ferroelectric Memristive Synapse for Back-End-of-Line Integration with Neuromorphic Hardware, *Adv. Electron. Mater.*, 2022, **8**(6), 2101395.

68 F. Xi, Y. Han, M. Liu, J. H. Bae, A. Tiedemann, D. Grützmacher and Q. T. Zhao, Artificial synapses based on ferroelectric Schottky barrier field-effect transistors for neuromorphic applications, *ACS Appl. Mater. Interfaces*, 2021, **13**(27), 32005–32012.

69 M. Halter, L. Bégon-Lours, M. Sousa, Y. Popoff, U. Drechsler, V. Bragaglia and B. J. Offrein, A multi-timescale synaptic weight based on ferroelectric hafnium zirconium oxide, *Commun. Mater.*, 2023, **4**(1), 14.

70 V. Mikheev, A. Chouprik, Y. Lebedinskii, S. Zarubin, Y. Matveyev, E. Kondratyuk, M. G. Kozodaev, A. M. Markeev, A. Zenkevich and D. Negrov, Ferroelectric second-order memristor, *ACS Appl. Mater. Interfaces*, 2019, **11**(35), 32108–32114.

71 S. S. Cheema, N. Shanker, S. L. Hsu, Y. Rho, C. H. Hsu, V. A. Stoica, Z. Zhang, J. W. Freeland, P. Shafer, C. P. Grigoropoulos and J. Ciston, Emergent ferroelectricity in subnanometer binary oxide films on silicon, *Science*, 2022, **376**(6593), 648–652.

72 Z. Fan, J. Deng, J. Wang, Z. Liu, P. Yang, J. Xiao, X. Yan, Z. Dong, J. Wang and J. Chen, Ferroelectricity emerging in strained (111)-textured ZrO_2 thin films, *Appl. Phys. Lett.*, 2016, **108**(1), 012906.

73 G. Antoniou, N. R. Halcovitch, M. Mucientes, W. I. Milne, A. Nathan, J. L. MacManus-Driscoll, O. V. Kolosov and G. Adamopoulos, Solution-processed thin film transistors incorporating YSZ gate dielectrics processed at 400 °C, *APL Mater.*, 2022, **10**(3), 031109.

74 K. Ferri, S. Bachu, W. Zhu, M. Imperatore, J. Hayden, N. Alem, N. Giebink, S. Trolier-McKinstry and J. P. Maria, Ferroelectrics everywhere: Ferroelectricity in magnesium substituted zinc oxide thin films, *J. Appl. Phys.*, 2021, **130**(4), 044101.

75 H. Moriwake, A. Konishi, T. Ogawa, K. Fujimura, C. A. Fisher, A. Kuwabara, T. Shimizu, S. Yasui and M. Itoh, Ferroelectricity in wurtzite structure simple chalcogenide, *Appl. Phys. Lett.*, 2014, **104**(24), 242909.

76 S. Lee, Y. Lee, D. Young Kim and T. Won Kang, Effects of Ti additives on structural and electric properties of Cr-and Ti-codoped ZnO layers, *J. Appl. Phys.*, 2013, **114**(6), 064102.

77 Y. C. Yang, C. Song, F. Zeng, F. Pan, Y. N. Xie and T. Liu, V^{5+} ionic displacement induced ferroelectric behavior in V-doped ZnO films, *Appl. Phys. Lett.*, 2007, **90**(24), 242903.

78 D. Dhananjay, J. Nagaraju and S. B. Krupanidhi, Off-centered polarization and ferroelectric phase transition in Li-doped ZnO thin films grown by pulsed-laser ablation, *J. Appl. Phys.*, 2007, **101**(10), 104104.

79 A. O. A. Onodera, N. T. N. Tamaki, Y. K. Y. Kawamura, T. S. T. Sawada and H. Y. H. Yamashita, Dielectric activity and ferroelectricity in piezoelectric semiconductor Li-doped ZnO, *Jpn. J. Appl. Phys.*, 1996, **35**(9S), 5160.

80 H. Zhang, A. Alanthattil, R. F. Webster, D. Zhang, M. B. Ghasemian, R. B. Venkataramana, J. Seidel and P. Sharma, Robust Switchable Polarization and Coupled Electronic Characteristics of Magnesium-Doped Zinc Oxide, *ACS Nano*, 2023, **17**(17), 17148–17157.

81 L. Jacques, G. Ryu, D. Goodling, S. Bachu, R. Taheri, P. Yousefian, S. Shetty, B. Akkopru-Akgun, C. Randall, N. Alem and J. P. Maria, Wake up and retention in zinc magnesium oxide ferroelectric films, *J. Appl. Phys.*, 2023, **133**(22), 224102.

82 K. Ferri, S. Bachu, W. Zhu, M. Imperatore, J. Hayden, N. Alem, N. Giebink, S. Trolier-McKinstry and J. P. Maria, Ferroelectrics everywhere: Ferroelectricity in magnesium substituted zinc oxide thin films, *J. Appl. Phys.*, 2021, **130**(4), 044101.

83 A. Konishi, T. Ogawa, C. A. Fisher, A. Kuwabara, T. Shimizu, S. Yasui, M. Itoh and H. Moriwake, Mechanism of polarization switching in wurtzite-structured zinc oxide thin films, *Appl. Phys. Lett.*, 2016, **109**(10), 102903.

84 S. Fichtner, N. Wolff, F. Lofink, L. Kienle and B. Wagner, AlScN: A III–V semiconductor based ferroelectric, *J. Appl. Phys.*, 2019, **125**(11), 114103.

85 F. Bernardini, V. Fiorentini and D. Vanderbilt, Spontaneous polarization and piezoelectric constants of III–V nitrides, *Phys. Rev. B*, 1997, **56**(16), R10024.

86 F. Tasnádi, B. Alling, C. Höglund, G. Wingqvist, J. Birch, L. Hultman and I. A. Abrikosov, Origin of the anomalous piezoelectric response in wurtzite $Sc_xAl_{1-x}N$ alloys, *Phys. Rev. Lett.*, 2010, **104**(13), 137601.

87 S. Zhang, D. Holec, W. Y. Fu, C. J. Humphreys and M. A. Moram, Tunable optoelectronic and ferroelectric properties in Sc-based III-nitrides, *J. Appl. Phys.*, 2013, **114**(13), 133510.

88 N. Farrer and L. Bellaiche, Properties of hexagonal ScN *versus* wurtzite GaN and InN, *Phys. Rev. B*, 2002, **66**(20), 201203.

89 D. Wang, J. Zheng, Z. Tang, M. D'Agati, P. S. Gharavi, X. Liu, D. Jariwala, E. A. Stach, R. H. Olsson, V. Roebisch and M. Kratzer, 2020, July. Ferroelectric c-axis textured aluminum scandium nitride thin films of 100 nm thickness. In 2020 Joint Conference of the IEEE International Frequency Control Symposium and International Symposium on Applications of Ferroelectrics (IFCS-ISAF) (pp. 1-4). IEEE.

90 D. Wang, J. Zheng, P. Musavigharavi, W. Zhu, A. C. Foucher, S. E. Trolier-McKinstry, E. A. Stach and

R. H. Olsson, Ferroelectric switching in sub-20 nm aluminum scandium nitride thin films, *IEEE Electron Device Lett.*, 2020, **41**(12), 1774–1777.

91 S. Yasuoka, T. Shimizu, A. Tateyama, M. Uehara, H. Yamada, M. Akiyama, Y. Hiranaga, Y. Cho and H. Funakubo, Effects of deposition conditions on the ferroelectric properties of $(Al_{1-x}Scx)$ N thin films, *J. Appl. Phys.*, 2020, **128**(11), 114103.

92 D. Wang, P. Wang, S. Mondal, M. Hu, Y. Wu, T. Ma and Z. Mi, Ultrathin Nitride Ferroic Memory with Large ON/OFF Ratios for Analog In-Memory Computing, *Adv. Mater.*, 2023, **35**(20), 2210628.

93 C. A. P. de Araujo, J. D. Cuchiaro, L. D. McMillan, M. C. Scott and J. F. Scott, Fatigue-free ferroelectric capacitors with platinum electrodes, *Nature*, 1995, **374**(6523), 627–629.

94 B. H. Park, B. S. Kang, S. D. Bu, T. W. Noh, J. Lee and W. Jo, Lanthanum-substituted bismuth titanate for use in non-volatile memories, *Nature*, 1999, **401**(6754), 682–684.

95 L. Li, P. Boullay, P. Lu, X. Wang, J. Jian, J. Huang, X. Gao, S. Misra, W. Zhang, O. Perez and G. Steciuk, Novel layered supercell structure from Bi_2AlMnO_6 for multifunctionalities, *Nano Lett.*, 2017, **17**(11), 6575–6582.

96 L. Li, P. Boullay, J. Cheng, P. Lu, X. Wang, G. Steciuk, J. Huang, J. Jian, X. Gao, B. Zhang and S. Misra, Self-assembled two-dimensional layered oxide supercells with modulated layer stacking and tunable physical properties, *Mater. Today Nano*, 2019, **6**, 100037.

97 H. Irie, M. Miyayama and T. Kudo, Structure dependence of ferroelectric properties of bismuth layer-structured ferroelectric single crystals, *J. Appl. Phys.*, 2001, **90**(8), 4089–4094.

98 Z. Tao, F. Che, F. Han, F. Wang, Z. Yang, W. Qi, Y. Wu and K. Zhang, Out-of-plane and In-plane piezoelectric behaviors of $[Ba (Zr_{0.2}Ti_{0.8})O_3]–0.5(Ba_{0.7}Ca_{0.3}TiO_3)$ thin films, *Prog. Nat. Sci.: Mater. Int.*, 2017, **27**(6), 664–668.

99 Q. Yang, J. Hu, Y. W. Fang, Y. Jia, R. Yang, S. Deng, Y. Lu, O. Dieguez, L. Fan, D. Zheng and X. Zhang, Ferroelectricity in layered bismuth oxide down to 1 nanometer, *Science*, 2023, **379**(6638), 1218–1224.

100 K. Yao, S. Chen, S. C. Lai and Y. M. Yousry, Enabling distributed intelligence with ferroelectric multifunctionalities, *Adv. Sci.*, 2022, **9**(1), 2103842.

101 A. R. Jayakrishnan, J. P. Silva, K. Gwozdz, M. J. Gomes, R. L. Hoye and J. L. MacManus-Driscoll, The Ferro-Pyro-Phototronic Effect for High-Performance Self-Powered Photodetectors, *Nano Energy*, 2023, 108969.

102 A. R. Jayakrishnan, A. Kumar, S. Druvakumar, R. John, M. Sudeesh, V. S. Puli, J. P. Silva, M. J. Gomes and K. C. Sekhar, Inorganic ferroelectric thin films and their composites for flexible electronic and energy device applications: current progress and perspectives, *J. Mater. Chem. C*, 2023, **11**, 827–858.

103 A. R. Jayakrishnan, J. P. Silva, K. Gwozdz, M. J. Gomes, R. L. Hoye and J. L. MacManus-Driscoll, The Ferro-Pyro-Phototronic Effect for High-Performance Self-Powered Photodetectors, *Nano Energy*, 2023, 108969.

104 J. P. Silva, K. C. Sekhar, H. Pan, J. L. MacManus-Driscoll and M. Pereira, Advances in dielectric thin films for energy storage applications, revealing the promise of group IV binary oxides, *ACS Energy Lett.*, 2021, **6**(6), 2208–2217.

105 A. R. Jayakrishnan, J. P. B. Silva, K. Kamakshi, D. Dastan, V. Annapureddy, M. Pereira and K. C. Sekhar, Are lead-free relaxor ferroelectric materials the most promising candidates for energy storage capacitors?, *Prog. Mater. Sci.*, 2022, 101046.